



Cite this: DOI: 10.1039/c8dt01285g

# Complete charge separation provoked by full cation encapsulation in the radical mono- and di-anions of 5,6:11,12-di-*o*-phenylene-tetracene†

Tobias Wombacher,<sup>a</sup> Richard Goddard,<sup>b</sup> Christian W. Lehmann<sup>b</sup> and Jörg J. Schneider<sup>a\*</sup>

Herein, we report the synthesis and molecular structure of the mono- and dianionic aromatic molecules [(B15C5-κ<sup>5</sup>O)<sub>2</sub>K<sup>+</sup>](L<sub>DOPT</sub><sup>•-</sup>) (**1**) and [(B15C5-κ<sup>5</sup>O)<sub>2</sub>K<sup>+</sup>]<sub>2</sub>(L<sub>DOPT</sub><sup>2-</sup>)THF<sub>solv</sub> (**2**) derived from the parent aromatic polyhydrocarbon 5,6:11,12-di-*o*-phenylenetetracene (DOPT, L<sub>DOPT</sub>) by a controlled stepwise one and two electron chemical reduction. The effect of single and double electron charge transfer to a polycondensed aromatic hydrocarbon (PAH) without any disturbing influence of an associated metal cation has been demonstrated. This was achieved by fully sandwiching the cationic K<sup>+</sup> counterions between two benzo-15-crown-5-ether (B15C5) ligands resulting in a fully encapsulating (κ<sup>10</sup>O) geometry which ensures a complete separation of the K<sup>+</sup> counterions and the bare anionic PAH species [L<sub>DOPT</sub><sup>•-</sup>] and [L<sub>DOPT</sub><sup>2-</sup>]. The structural changes accompanied by the stepwise reduction from L<sub>DOPT</sub> to [L<sub>DOPT</sub><sup>•-</sup>] to [L<sub>DOPT</sub><sup>2-</sup>] are discussed and compared to earlier predictions based on density functional theory (DFT) as well as the results of previous studies of alkaline metal cationic PAH anion interactions of DOPT in which only a partial metal cation encapsulation has been achieved so far.

Received 2nd April 2018,  
Accepted 24th May 2018

DOI: 10.1039/c8dt01285g

rsc.li/dalton

## Introduction

During the last decade, a variety of alternant polynuclear aromatic hydrocarbon (PAH) species and derivatives thereof have been synthesized and studied in devices such as biosensors<sup>1,2</sup> or transistors.<sup>2-4</sup> Their remarkable capability of coordinating transition metals onto the π-perimeter framework makes them interesting molecules for deployment in the field of catalysis or as building blocks in synthetic chemistry.<sup>5</sup> Electronic processes play an important role in both functional processes incorporating these in electronic devices<sup>4,6,7</sup> and chemical processes,<sup>8</sup> whereby the electron redistribution and the reactivity of the compounds are strongly influenced by the changing electron density distribution along the π-perimeter. A comparison of structural data of various PAH systems in the solid state with experimental results obtained from NMR, ESR or UV-vis measurements has revealed that in many cases the single

crystal structures of the charged and neutral compounds represent the species detectable in solution.<sup>9</sup> Recently, our group has been interested in the isolation of crystalline PAH anions of the newly accessible compound 5,6:11,12-di-*o*-phenylene-tetracene (DOPT, L<sub>DOPT</sub>) for which we have derived a scaled up multigram method for its synthesis.<sup>10</sup> This synthetic approach has allowed us to further unravel its so far unknown material properties<sup>4</sup> and reaction behavior.<sup>11,12</sup> In highly conjugated π-systems, any modification of the charge density (*e.g.* coordination, oxidation or reduction) generally influences the bonding situation and consequently affects the structural shape of the resulting molecule compared to its parent neutral state.<sup>13</sup> The degree of perturbation essentially depends on the type of PAH and is most distinctive for (i) structurally flexible π-compounds exhibiting adjacent alkyl or phenyl groups, such as 1,2-diphenylbenzene<sup>14</sup> or rubrene<sup>15</sup> and/or (ii) when an intrinsic contortion of the aromatic framework occurs, as in the case of half bowl-shaped corannulene<sup>16</sup> or nanobelts.<sup>17</sup>

Since these factors represent feasible changes in shape, they strongly contribute to the observed structural deformation upon reduction.<sup>13,18</sup> Despite the importance of redox changes in the overall structure of charged PAHs, such distortions are often solely discussed in terms of ion-pairs showing a strong (iii) electrostatic interaction.<sup>19</sup> In order to distinguish these effects, the groups of Bock *et al.*<sup>20-22</sup> and Petrukhina *et al.*<sup>16,23-25</sup> described solvent-separated PAH anions by

<sup>a</sup>Fachbereich Chemie, Eduard-Zintl-Institut für Anorganische und Physikalische Chemie, Alarich-Weiss Str. 12, 64287 Darmstadt, Germany.

E-mail: joerg.schneider@ac.chemie.tu-darmstadt.de

<sup>b</sup>Max-Planck-Institut für Kohlenforschung, Kaiser-Wilhelm-Platz 1, 45470 Mülheim an der Ruhr, Germany

† Electronic supplementary information (ESI) available. CCDC 1820791 (**1**) and 1820792 (**2**). For ESI and crystallographic data in CIF or other electronic format see DOI: 10.1039/c8dt01285g

masking the counter-ion partly with suitable open-chain polyethers or encapsulating crown-ethers. Examples of structural changes in the mono and dianions of the PAHs decacylene ( $L_{Dec}$ ), pentacene ( $L_{Pent}$ ) and perylene ( $L_{Pery}$ ) are revealed in the molecular structures  $[(\text{triglyme-}\kappa^4\text{O})_3\text{Cs}^+](L_{Dec}^{2-})$ ,<sup>26</sup>  $[(\text{DME-}\kappa^2\text{O})_3\text{Na}^+]_2(L_{Pent}^{2-})$ <sup>26</sup> and  $[(\text{diglyme-}\kappa^3\text{O})_2\text{Na}^+]_2(L_{Pery}^{2-})$ .<sup>27</sup> Remarkably and to the best of our knowledge, no systematic studies on the influence of electrostatic interactions in a family of PAH anions in solvent-separated ion-pairs were undertaken until our recent report<sup>12</sup> in which we presented dianionic structures featuring the DOPT dianion framework. In this investigation, the significant and sole influence of the counter cationic charge on the shape of the charged PAH was exemplified in the solvent-separated *naked* ion pairs  $[(\text{DME-}\kappa^2\text{O})_3\text{Li}^+]_2(L_{DOPT}^{2-})$  (3),  $[(\text{DME-}\kappa^2\text{O})_3\text{Na}^+]_2(L_{DOPT}^{2-})$  (4) and  $[(\text{diglyme-}\kappa^3\text{O})_2\text{Na}^+]_2(L_{DOPT}^{2-})$  (5). With an increase in the size of the alkaline metal cation and its surrounding polyether shell, the distance between the countercharges increased and deformation of the dianionic  $\pi$ -perimeter was progressively reduced going from 3 to 5. Nonetheless, a significant structural perturbation within  $[L_{DOPT}^{2-}]$  was still observable, accompanied by a significant deviation from the planar symmetry of the parent neutral DOPT. In completion of this work, we now present our investigations into the fully naked PAH anions of DOPT obtained by complete encapsulation and thus shielding of the respective metal cation whereby a complete suppression of anion/cation electrostatic interaction has been brought about by strict separation of the individual countercharges.

## Results and discussion

The prototype of a naked anionic aromatic ligand is the free cyclopentadienide ( $L_{CP}$ ) anion, which has been crystallized as its tetraethylammonium, methyltriphenylphosphonium, dimethyl-diphenylphosphonium and tetraethylphosphonium salts,<sup>28</sup> tetra-*n*-butylammonium salt,<sup>29</sup> its tetraphenylphosphonium salt<sup>30</sup> and its potassium salt  $[(15\text{C5-}\kappa^5\text{O})_2\text{K}^+](L_{CP}^-)$  by utilizing the oxygen macrocycle 15-crown-5-ether (15C5) to encapsulate and isolate the potassium cation.<sup>31</sup> In this work, we have systematically decreased the electrostatic interaction between the anion and cation ( $[(L_{DOPT}^{n-x-})][x\text{K}^+]$ ;  $n = 0, 1$ ;  $x = 1, 2$ ) by coordinating the alkali metal to the benzo-oxygen 15-crown-5-ether oxygen macrocycle. We found that as a result of the large distance between the anion and the cation, the electrostatic interaction between the cationic countercharges is almost completely suppressed, thus allowing the fully naked  $[L_{DOPT}^{n-x-}]$  molecule to be isolated. Correlation of the crystallographic data of neutral and anionic DOPT with DFT calculations of their frontier orbitals provides insight into the concept of complete charge separation within such ion couples (see ESI†).<sup>32</sup> Due to the strong affinity of the poly-*O*-macrocycle benzo-15-crown-5-ether (B15C5) for  $\text{K}^+$  as shown for the crystalline ion pair  $\{[(\text{B15C5-}\kappa^5\text{O})_2\text{K}^+](\text{I}^-)\}$ ,<sup>33</sup> we chose this crown-ether to fully complex the metal.

## Synthesis and molecular structure of the potassium compound $[(\text{B15C5-}\kappa^5\text{O})_2\text{K}^+](L_{DOPT}^-)$ (1)

$[(\text{B15C5-}\kappa^5\text{O})_2\text{K}^+](L_{DOPT}^-)$  (1) was obtained by a reaction of  $L_{DOPT}$  with one equivalent of potassium metal in dry THF at ambient temperature. The addition of two equivalents of dried B15C5 yielded exclusively 1 as dark-green rhomboids in high yield, suitable for X-ray analysis. Crystals of 1 are highly sensitive to air and moisture which makes a stringent pre-drying of all gases and solvents used absolutely necessary. So far, this sensitivity has precluded any spectroscopic characterisation. The solvent-separated ion-pair crystallizes in the triclinic space group  $P\bar{1}$  (no. 2) with two formula units in the cell (Fig. 2 and Table 1). Notably, 1 is one of the rare cases of a structurally characterized PAH monoanion. PAH monoanions mainly occur as half-solvated contact-ion-pairs. Among those are, for example, the radical monoanions of 1,3,5-triphenylbenzene,<sup>34</sup> naphthalene<sup>35,36</sup> and (9,10-diphenyl)anthracene,<sup>35,37,38</sup> dibenzo-*[a,e]*pentalene,<sup>39</sup> biphenylene,<sup>40</sup> fluoranthene,<sup>41</sup> perylene,<sup>9</sup> pyrene<sup>42</sup> and rubrene,<sup>13</sup> originating from the research groups of Bock<sup>9,18,35,37,38,40,43-45</sup> and Petrukhina<sup>13,16,46</sup>.

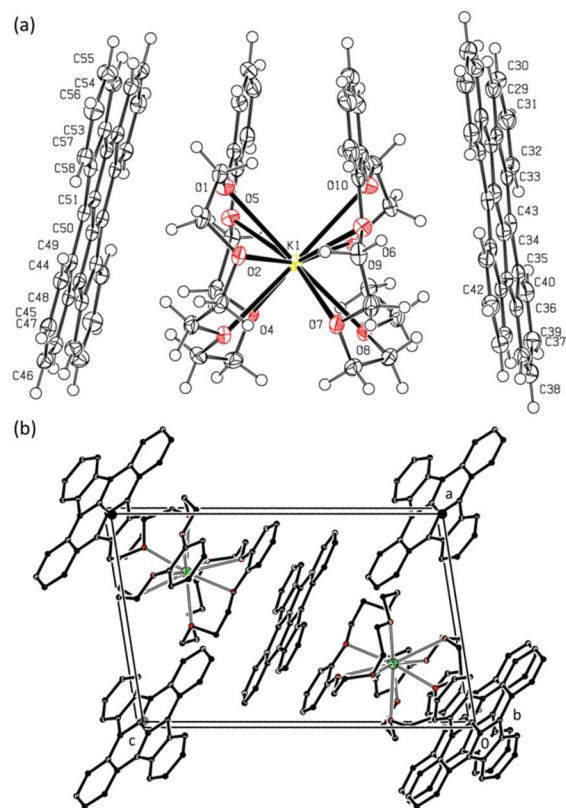


**Fig. 1** (a) ORTEP<sup>47</sup> plot of the molecular structure of  $[(\text{B15C5-}\kappa^5\text{O})_2\text{K}^+](L_{DOPT}^-)$  (1) drawn at the 50% probability level. (b) View of the unit cell of 1. Each unit cell contains two molecules of  $[L_{DOPT}^-]$  (one complete molecule in the center and four fragments on the edges of the cell) and two  $[(\text{B15C5-}\kappa^5\text{O})_2\text{K}^+]$  molecules. Within the  $[(\text{B15C5-}\kappa^5\text{O})_2\text{K}^+]$  molecule, the 1,2-phenylene-groups of each B15C5 ligand adopt a staggered arrangement around the K atom. Hydrogen atoms are omitted for clarity.

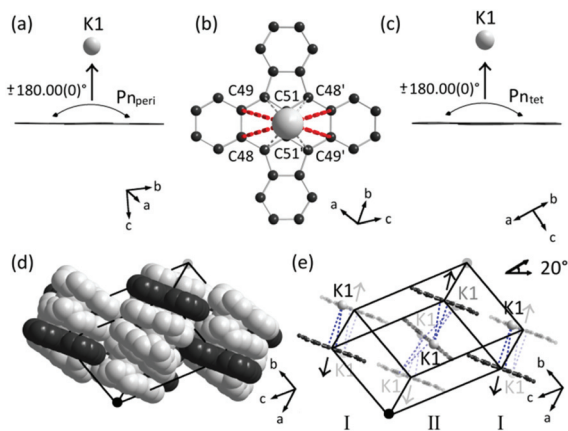


**Fig. 2** Illustration of the structural motifs found in compound **1**. (a, c) Full planarity is found for  $[L_{DOPT}^{\cdot-}]$ , (b) orientation of the encapsulated  $K^+$  atop and below the central naphthacenic unit. Long-range distances  $d(K \cdots C_{\pi})$  (red) to the naphthacenic core are  $d(K \cdots C_{\pi}) = 625\text{--}640$  pm for C48–C49/C48'–C49'. (d) Space-filling model showing the dense packing motif. The small inclination by *ca.*  $\angle 13^\circ$  of both encapsulating B15C5 ligands within a  $[(B15C5-\kappa^5O)_2K^+]$  unit is highlighted in light grey. (e) Isolated  $[L_{DOPT}^{\cdot-}]$  units adopt a herringbone type arrangement with an inclination angle of  $\angle 20^\circ$  between I and II. Closest distances of the charged  $\pi$ -perimeter to nearby counterions are given in blue:  $d(K \cdots C_{\pi}) = 582/585$  pm for C51/C51'.

Recently, Petrukhina *et al.* obtained the first solvent-separated radical monoanions of bowl-shaped corannulene ( $L_{Corra}$ ) in the form of  $\{[(18C6-\kappa^6O)Na^+](L_{Corra}^{\cdot-})\}$ ,<sup>16</sup>  $\{[(18C6-\kappa^6O)(THF-\kappa^1O)_2Na^+](L_{Corra}^{\cdot-})\}$ <sup>16</sup> and  $\{[(DME-\kappa^2O)_3Na^+](L_{Corra}^{\cdot-})\}$ <sup>46</sup> and coronene ( $L_{Coro}$ ) in  $\{[(DME-\kappa^2O)_3Na^+](L_{Coro}^{\cdot-})\}$ .<sup>46</sup>

The crown-ether encapsulated potassium ions of **1** are located above and below the central  $C_{\pi}-C_{\pi}$ -bond (C51–C51') of  $[L_{DOPT}^{\cdot-}]$  with  $d(M \cdots C_{\pi})_1 = 582\text{--}640$  pm (Fig. 2b). The completely planar geometry observed in the parent neutral DOPT molecule is fully conserved in its radical monoanion (see Fig. 2a and c).

Within the  $[(B15C5-\kappa^5O)_2K^+]$  capsules, both B15C5 ligands are tilted by *ca.*  $\angle 13^\circ$  (Fig. 2d) with respect to the 1,2-phenylene ring planes. A metal-to-oxygen distance of  $\bar{d}(M-O)_1 = 289$  pm is observed for all oxygen atoms of the two polyether ligands indicating that they contribute equally to the overall shielding of the +1 charge. The individual anion molecules  $[L_{DOPT}^{\cdot-}]$  are oriented in a herringbone type arrangement with an inclination angle of  $\angle 20^\circ$  between the mean planes of the radicals (Fig. 2e). This motif results in the formation of infinite stacks with the sequence  $[L_{DOPT}^{\cdot-}] \cdots [(B15C5-\kappa^5O)_2K^+] \cdots [L_{DOPT}^{\cdot-}]_{II}$  oriented in parallel along the diagonal of the unit cell along the  $[\bar{1}11]$  direction.

### Synthesis and molecular structure of the dipotassium compound $[(B15C5-\kappa^5O)_2K^+]_2(L_{DOPT}^{2-})THF_{solv}$ (**2**)

Employing the same procedure but using two equivalents of potassium metal followed by addition of four equivalents of B15C5 affords the almost quantitative precipitation again as highly air and moisture sensitive solvent-separated ion-pair

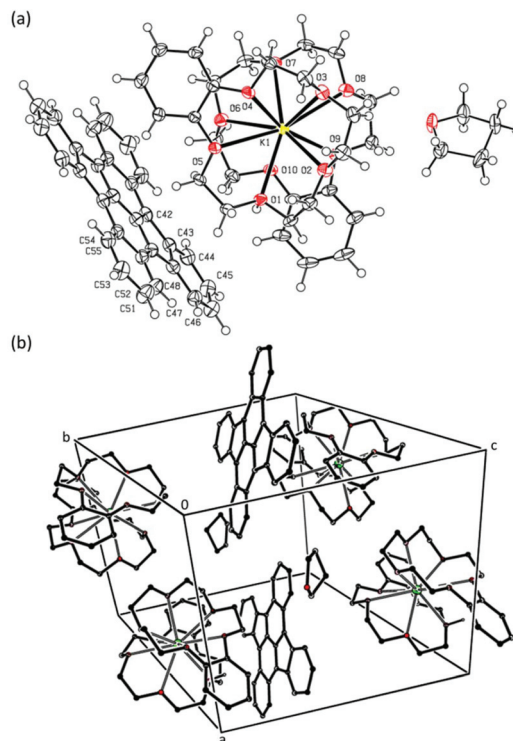


**Fig. 3** (a) ORTEP<sup>47</sup> plot of the molecular structure of  $[(B15C5-\kappa^5O)_2K^+]_2(L_{DOPT}^{2-})THF_{solv}$  (**2**) drawn at the 50% probability level showing the major component of the slightly disordered THF molecule. (b) View of the unit cell of **2**. Each aromatic molecule of  $[L_{DOPT}^{2-}]$  is positioned along the center of the (*b*–*c*) plane and sandwiched by two cationic molecules of  $[(B15C5-\kappa^5O)_2K^+]$  within the (*a*–*b*) plane. THF occupies free lattice positions between the separated ion-pairs along a corridor through the center of the (*a*–*c*) plane. The 1,2-phenylene groups of B15C5 are staggered by  $140^\circ$ , deviating strongly from conformation adopted by the radical monoanion **1**:  $50^\circ$ ;  $\Delta = 90^\circ$  vs.  $[(B15C5-\kappa^5O)_2K^+]^-$ :<sup>29</sup>  $0^\circ$ ;  $\Delta = 140^\circ$ . Each unit cell contains one molecule of  $[L_{DOPT}^{2-}]$  ( $2 \times \frac{1}{2}L_{DOPT}^{2-}$ ), two molecules of  $[(B15C5-\kappa^5O)_2K^+]$  ( $4 \times \frac{1}{2}[(B15C5-\kappa^5O)_2K^+]$ ) and one THF molecule ( $2 \times \frac{1}{2}THF$ ). Hydrogen atoms are omitted for clarity.

$[(B15C5-\kappa^5O)_2K^+]_2(L_{DOPT}^{2-})THF_{solv}$  (**2**), this time as highly air sensitive deep red rhombic crystals. Notably, the pronounced color change from blue *via* green to deep red ( $L_{DOPT} \rightarrow \mathbf{1} \rightarrow \mathbf{2}$ ) clearly reflects the ongoing reduction reaction, which is clearly visible to the naked eye. **2** crystallizes in the triclinic space group  $P\bar{1}$  (no. 2) with one formula unit in the cell (Fig. 3 and Table 1).

The dianionic  $\pi$ -perimeter  $[L_{DOPT}^{2-}]$  is as far as can be ascertained planar with a negligible twist of the peripheral phenylene rings ( $Pn_{peri}$ ) (Fig. 4a and c). Each  $[L_{DOPT}^{2-}]$  dianion is accompanied by two  $[(B15C5-\kappa^5O)_2K^+]$  capsules, one above and one below the five membered ring positions of the major component [87.7(3)%] with  $d(M \cdots C_{\pi})_2 = 646\text{--}670$  pm. Presumably, owing to packing effects in the crystal lattice, these distances are slightly larger than those observed for the radical monoanion **1** ( $d(M \cdots C_{\pi})_1 = 582\text{--}640$  pm), whereas the average metal to oxygen distance of  $\bar{d}(M-O)_2 = 289$  pm =  $\bar{d}(M-O)_1$  remains the same. This suggests that the shielding of the

Table 1 Crystallographic data for neutral DOPT and its anionic compounds 1–5 are summarized together with the respective type of each ion encapsulating the poly-O ligand shell

Substance	1	2	3 <sup>12</sup>	4 <sup>12</sup>	5 <sup>12</sup>
Type of capsule	None	[(B15C5-κ <sup>5</sup> O) <sub>5</sub> K <sup>+</sup> ] <sub>2</sub>	[(DME-κ <sup>2</sup> O) <sub>3</sub> Li <sup>+</sup> ] <sub>2</sub>	[(DME-κ <sup>2</sup> O) <sub>3</sub> Na <sup>+</sup> ] <sub>2</sub>	[[diglyme-κ <sup>3</sup> O) <sub>2</sub> Na <sup>+</sup> ] <sub>2</sub>
Crystal size [mm <sup>3</sup> ]	0.440 × 0.280 × 0.200	0.23 × 0.19 × 0.07	0.28 × 0.24 × 0.15	0.312 × 0.117 × 0.099	0.614 × 0.593 × 0.533
Crystal system	Monoclinic	Triclinic	Triclinic	Triclinic	Monoclinic
Space group, Z	C2/c (no. 15), Z = 4	P $\bar{1}$ (no. 2), Z = 1	P $\bar{1}$ (no. 2), Z = 4	P $\bar{1}$ (no. 2), Z = 4	P2 <sub>1</sub> /n (no. 14), Z = 2
Unit cell	a = 24.802(5) Å b = 3.8834(6) Å c = 21.100(4) Å β = 119.40(3)°	a = 11.0923(3) Å b = 13.0606(3) Å c = 16.7307(4) Å α = 82.9084(10)° β = 80.2410(9)° γ = 76.9312(10)°	a = 12.746(7) Å b = 13.528(3) Å c = 13.986(4) Å α = 66.815(4)° β = 89.408(4)° γ = 88.240(5)°	a = 13.369(3) Å b = 18.451(4) Å c = 23.373(5) Å α = 67.147(4)° β = 89.198(4)° γ = 88.091(4)°	a = 12.101(2) Å b = 13.542(2) Å c = 15.849(3) Å β = 102.704(3)°
V	1770.5(7) Å <sup>3</sup>	2317.70(10) Å <sup>3</sup>	5198(2) Å <sup>3</sup>	5310(2) Å <sup>3</sup>	2533.7(8) Å <sup>3</sup>
Emp. formula	C <sub>30</sub> H <sub>16</sub>	C <sub>54</sub> H <sub>112</sub> K <sub>2</sub> O <sub>21</sub>	C <sub>54</sub> H <sub>76</sub> Li <sub>2</sub> O <sub>12</sub>	C <sub>54</sub> H <sub>61</sub> O <sub>11.78</sub>	C <sub>54</sub> H <sub>72</sub> Na <sub>2</sub> O <sub>12</sub>
Formula weight	376.43 g mol <sup>-1</sup>	1672.03 g mol <sup>-1</sup>	931.02 g mol <sup>-1</sup>	956.53 g mol <sup>-1</sup>	959.09 g mol <sup>-1</sup>
Density (calc.)	1.412 g cm <sup>-3</sup>	1.323 g cm <sup>-3</sup>	1.190 g cm <sup>-3</sup>	1.197 g cm <sup>-3</sup>	1.257 g cm <sup>-3</sup>
Abs. coefficient	0.080 mm <sup>-1</sup>	0.189 mm <sup>-1</sup>	0.082 mm <sup>-1</sup>	0.097 mm <sup>-1</sup>	0.102 mm <sup>-1</sup>
F(000)	784 e	890 e	2008 e	2029 e	1028 e
θ range	3.306 to 25.333°	2.69 to 67.49°	1.212 to 26.372°	1.524 to 23.256°	2.635 to 37.597°
Index ranges	-29/29, -4/4, -25/14	-13/13, -15/15, -19/19	-16/16, -22/22, -28/28	-14/14, -20/20, -25/25	-20/20, -23/23, -26/26
Coll. reflections	4789	55 453	104 116	82 306	256 525
Ind. reflections	1612 [R(int) = 0.0264]	8049 [R(int) = 0.0358]	21 135 [R(int) = 0.0817]	15 224 [R(int) = 0.1154]	13 081 [R(int) = 0.0595]
Completeness	99.3%	96.3%	99.7%	99.9%	99.9%
Obsd	[I > 2σ(I)]	[I > 2σ(I)]	[I > 2σ(I)]	[I > 2σ(I)]	[I > 2σ(I)]
Reflections used for refinement	1612	8049	21 135	10 180	10 334
Abs. correction	Semi-empirical from equivalents	Gaussian	Semi-empirical from equivalents	Semi-empirical from equivalents	Semi-empirical from equivalents
Largest difference peak and hole	0.250/-0.202 e Å <sup>3</sup>	0.18/-0.26 e Å <sup>3</sup>	0.89/-0.43 e Å <sup>3</sup>	0.728/-0.707 e Å <sup>3</sup>	1.090/-0.546 e Å <sup>3</sup>
Treatment of hydrogen atoms	Positioned geometrically	Positioned geometrically	Positioned geometrically	Positioned geometrically	Positioned geometrically
Refined param.	136	622	1250	1256	331
GOF on F <sup>2</sup>	1.136	0.969	1.068	1.246	1.052
wR <sub>2</sub> (all data)	0.1297	0.0788	0.3383	0.3156	0.1546
R <sub>1</sub> [I > 2σ(I)]	0.0517	0.0319	0.1058	0.1065	0.0534

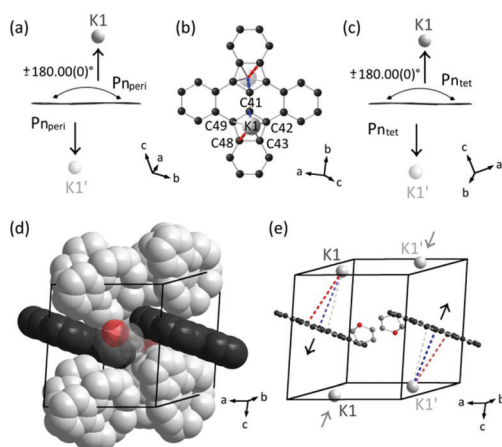


**Fig. 4** Detailed representation of the structural motifs found in **2**. (a, c) The plane of  $[\text{LDOPT}^{2-}]$  is planar, (b) with both  $[(\text{B15C5-}\kappa^5\text{O})_2\text{K}^+]$  units located above and below the centers of the five-membered rings with  $d(\text{M}\cdots\text{C}_\pi) = 646\text{--}670$  pm towards C41 (blue) and C48 (red). (d, e) The 1,2-phenylene rings of each B15C5 ligand are inclined by only *ca.*  $\angle 2^\circ$  within a  $[(\text{B15C5-}\kappa^5\text{O})_2\text{K}^+]$  unit. The stacking of both B15C5 ligands by  $140^\circ$  results in an oval shape of the  $[(\text{B15C5-}\kappa^5\text{O})_2\text{K}^+]$  units and in the formation of free cavities in the crystal lattice occupied by isolated solvent molecules of THF (red). (e) Large surface area interaction between cation and anion in **2**.

potassium ion is similar in **1** and **2**. Within the  $[(\text{B15C5-}\kappa^5\text{O})_2\text{K}^+]$  molecules, the centroids of the 1,2-phenylene groups make a torsion angle about the centroids of the two pairs of O atoms of  $135^\circ$ , resulting in an oval shape of the enclosing ligand shell for **2**, enabling a large surface area interaction between the ions. THF molecules arranged along the  $[010]$  direction fill the voids between the ion triads.

The planar geometry that is observed in the parent neutral DOPT is fully conserved in both anionic molecules  $[(\text{B15C5-}\kappa^5\text{O})_2\text{K}^+](\text{LDOPT}^{2-})$  (**1**) and  $[(\text{B15C5-}\kappa^5\text{O})_2\text{K}^+]_2(\text{LDOPT}^{2-})\text{THF}_{\text{solv}}$  (**2**). Remarkably, this is in stark contrast to the previously presented ion pairs  $[(\text{DME-}\kappa^2\text{O})_3\text{Li}^+]_2(\text{LDOPT}^{2-})$  (**3**),  $[(\text{DME-}\kappa^2\text{O})_3\text{Na}^+]_2(\text{LDOPT}^{2-})$  (**4**) and  $\{[(\text{diglyme-}\kappa^3\text{O})_2\text{Na}^+]_2(\text{LDOPT}^{2-})\}$  (**5**)<sup>12</sup> (crystallographic data for DOPT and compounds **1–5**<sup>12</sup> are given in Table 1 for comparison).

### Structural comparison to recently synthesized compounds within the alkali metal series of DOPT anions

A detailed summary of the extent of the  $\pi$ -deformation in the alkali metal salts of DOPT ( $\text{Li}^+ \rightarrow \text{Cs}^+$ ) known so far is given in Fig. 5. For completeness, this also includes the recently reported heavier congeners containing  $\text{Rb}^+$  and  $\text{Cs}^+$   $\{[(\text{18C6-}\kappa^6\text{O})\text{Rb}^+]_2-\mu-(\eta^6:\eta^6-\text{LDOPT}^{2-})\}$   $\{[(\text{18C6-}\kappa^6\text{O})\text{Rb}^+]_2-\mu-(\eta^4:\eta^4-\text{LDOPT}^{2-})\}$   $(\text{THF}_{\text{solv}})_2$  (**6**)<sup>11</sup> and  $[\mu-(\eta^4:\eta^4-\text{LDOPT}^{2-})]_{0.5}(\text{tetraglyme-}\kappa^4\text{O})(\text{tetraglyme-}\kappa^2\text{O})\text{Cs}^+]_2-\mu-(\eta^2:\eta^2-\text{LDOPT}^{2-})_{0.5}]_n$  (**7**)<sup>11</sup>. A comparison of the structural parameters of all the so far structurally characterized solvent-separated ion-pairs of DOPT (**1–5**) reveals different trends, which substantiate the view that there is a maximum in charge separation for **1** and **2** compared to the dianions **3–5** (Fig. 5a). Increasing size and electronic softness

(a) $\text{M}^+$	$x$	shape $[\text{LDOPT}^{n-x}]$	$d(\text{M}\cdots\text{C}_\pi)$	ligand	$\kappa^y$	$\bar{d}(\text{M-O})$	$\bar{d}(\kappa^y\text{O})$
<b>3</b>	$\text{Li}^+$	○ ○	535–577	DME	6	214	550
<b>4</b>	$\text{Na}^+$	● ●	543–586	DME	6	234	580
<b>5</b>	$\text{Na}^+$	● ●	547–570	diglyme	6	239	625
<b>1</b>	$\text{K}^+$	○ ○	582–640	B15C5	10	289	725
<b>2</b>	$\text{K}^+$	● ●	646–670	B15C5	10	289	725

(b) $\text{M}^+$	$x$	shape $[\text{LDOPT}^{n-x}]$	$d(\text{M-C}_\pi)$	ligand	$\kappa^x$	$\bar{d}(\text{M-O})$	$\bar{d}(\kappa^y\text{O})$
<b>6</b>	$\text{Rb}^+$	● ●	302–352	18C6	6	296	-
<b>7</b>	$\text{Cs}^+$	● ●	322–360	tetraglyme	6	314	-

**Fig. 5** (a) Characteristic structural details of solvent separated molecular structures of all anionic DOPT containing  $[\text{LDOPT}^{n-x}]$  molecules with  $n = 0, 1, 2$ . (†) A trend towards the planar fully naked DOPT anion is observed using potassium as a reducing agent in combination with two encapsulating B15C5 ligands in the  $(\kappa^{10}\text{O})$ -geometry. Metal to carbon distance ( $d(\text{M}\cdots\text{C}_\pi)$ ), median metal to oxygen distance ( $\bar{d}(\text{M-O})$ ) and median diameter of the ligand shell ( $\bar{d}(\kappa^y\text{O})$ ;  $y = 6, 10$ ) steadily increase along the series  $\text{Li}^+ < \text{Na}^+ < \text{K}^+$  and from DME  $\rightarrow$  diglyme  $\rightarrow$  B15C5 and from  $\kappa^6\text{O} \rightarrow \kappa^{10}\text{O}$ . (b) The corresponding  $\text{Rb}^+$  and  $\text{Cs}^+$  compounds  $\{[(\text{18C6-}\kappa^6\text{O})\text{Rb}^+]_2-\mu-(\eta^6:\eta^6-\text{LDOPT}^{2-})\}$   $\{[(\text{18C6-}\kappa^6\text{O})\text{Rb}^+]_2-\mu-(\eta^4:\eta^4-\text{LDOPT}^{2-})\}$   $(\text{THF}_{\text{solv}})_2$  (**6**)<sup>11</sup> and  $[\mu-(\eta^4:\eta^4-\text{LDOPT}^{2-})]_{0.5}(\text{tetraglyme-}\kappa^4\text{O})(\text{tetraglyme-}\kappa^2\text{O})\text{Cs}^+]_2-\mu-(\eta^2:\eta^2-\text{LDOPT}^{2-})_{0.5}]_n$  (**7**)<sup>11</sup> are listed for comparison. Both exhibit  $d(\text{M-C}_\pi)$  distances well below 360 pm and overall longer  $\bar{d}(\text{M-O})$  distances. (‡) A similar deformation of the  $\pi$ -perimeter is observed for the  $\text{Cs}^+$  compound **7** as for the solvent-separated  $\text{Na}^+$ -diglyme compound **5**, but with a strongly different perturbation of the electron distribution along the  $\pi$ -plane (see ESI†).

of the alkaline metal cations ( $\text{Li}^+ \rightarrow \text{K}^+$ ), the short metal to carbon distances  $d(\text{M}\cdots\text{C}_\pi)$  increases steadily ranging from 535–577 pm for  $\text{Li}^+$  up to 646–670 pm for  $\text{K}^+$ . This trend is also mirrored in the increasing size of the ether ligand shell  $\bar{d}(\kappa^y\text{O})$  distances (550 pm for  $\text{Li}^+\text{@DME} \rightarrow 725$  pm with  $\text{K}^+\text{@B15C5}$ ). Subsequently performed DFT calculations of the electrostatic potential surfaces of the different alkaline metal capsules confirm the results from the X-ray data (Fig. 6).

The molecular surface electrostatic potentials were all calculated at the B3LYP/6-31G\*\* level using  $0.002 \text{ e au}^{-3}$  as the contour of the electron density. Median values of the molecular surface electrostatic potentials were taken from 10 points along the periphery and then averaged to  $\bar{V}_s(r)$ .<sup>48,49</sup> Indeed, the predicted electrostatic potential along the periphery of the alkaline metal capsules is significantly diminished in going from  $[(\text{DME-}\kappa^2\text{O})_3\text{Li}^+]$  in **3** to  $[(\text{B15C5-}\kappa^5\text{O})_2\text{K}^+]$  in **1** and **2**, in accordance with the increased softness of  $\text{K}^+$  compared to  $\text{Li}^+$ .

Thus, the observed perturbation of the carbon skeleton decreases to a minimum for **1** and **2** containing  $\text{K}^+$  (see † in Fig. 5a). This trend is also reflected in the average metal-to-oxygen distance  $\bar{d}(\text{M-O})$  which increases from 214 pm to 289 pm and correlates with the increasing size and softness of the potassium ion ( $r(\text{Li}^+) = 76 \text{ pm} \ll r(\text{K}^+) = 138 \text{ pm}$  (ref. 51)). However, it is worth noting that the corresponding solvent shared ion-pairs containing  $\text{Rb}^+$  and  $\text{Cs}^+$  in **6** and **7** exhibit

only a slight deformation of the  $[L_{\text{DOPT}}^{2-}]$  carbon skeletons (Fig. 6b). Nonetheless, a strong electronic exchange between the countercharges predominantly determines the local electron concentration on the charged  $[L_{\text{DOPT}}^{2-}]$  ligand of these solvent-shared ion-pairs. To the best of our knowledge, **1** and **2** can be regarded as the first examples of a PAH containing fully naked anions.

Despite slight disorder of one of the  $[L_{\text{DOPT}}^{\cdot-}]$  radical anions [11.5(7)%] in the crystal structure of **1** and slight disorder of the  $[L_{\text{DOPT}}^{2-}]$  dianion in **2** [12.3(3)%], both anionic units of  $[L_{\text{DOPT}}^{\cdot-}]$  in **1** and  $[L_{\text{DOPT}}^{2-}]$  in **2** exhibit structural changes  $\Delta d_{\text{C-C}}$  (pm) upon reduction when compared to the parent neutral state (Fig. 5). Fig. 7 summarizes the observed changes  $\Delta d_{\text{C-C}}$  (pm) in the geometries of  $[L_{\text{DOPT}}^{\cdot-}]$  in **1** and  $[L_{\text{DOPT}}^{2-}]$  in **2** upon electron consumption compared to the parent neutral state (Fig. 7).

Reduction of DOPT to  $[L_{\text{DOPT}}^{\cdot-}]$  and subsequently to  $[L_{\text{DOPT}}^{2-}]$  transfers one, and two electrons respectively into the LUMO of DOPT while keeping the planarity of the  $\pi$ -system intact (Fig. 7a and b).<sup>4</sup> As a consequence, a major increase in

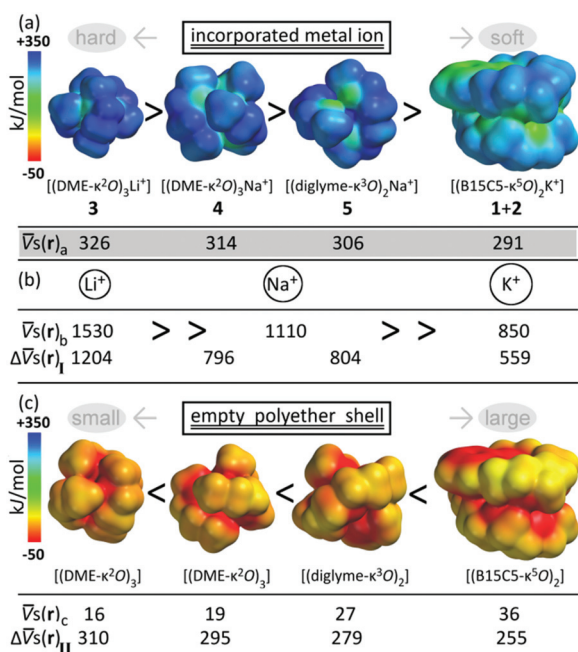


**Fig. 6** Electrostatic potential surfaces (kJ mol<sup>-1</sup>) calculated at the B3LYP/6-31G\*\* level of (a) the alkali metal capsules  $[(\text{DME}-\kappa^2\text{O})_3\text{Li}^+]$  of **3**,  $[(\text{DME}-\kappa^2\text{O})_3\text{Na}^+]$  of **4**,  $[(\text{diglyme}-\kappa^3\text{O})_2\text{Na}^+]$  of **5** and  $[(\text{B15C5}-\kappa^5\text{O})_2\text{K}^+]$  of **1** and **2**, (b) the bare metal ions and (c) its hypothetical metal-free state, together with the median values of the molecular surface electrostatic potential ( $\bar{V}_s(r)$ ) (red = low/negative potential, blue = high/positive potential according to Feldmann<sup>50</sup>). The differences in the electrostatic potential for the corresponding ligand capsules ( $\bar{V}_s(r)_a$ ) are given for comparison with the free ions ( $\bar{V}_s(r)_b$ ) and the empty polyether shell ( $\bar{V}_s(r)_c$ ), respectively. A decrease in  $\bar{V}_s(r)$  is observed towards the  $(\kappa^{10}\text{O})$ -geometry in compounds **1** and **2**. Notably, the major impact on the diminished electrostatic potential in  $[(\text{B15C5}-\kappa^5\text{O})_2\text{K}^+]$  arises from the increasing size of the crown-ether capsule and the decreasing potential of the encapsulated ion. Starting coordinates for the calculations were taken from the corresponding crystal structure data of **1**–**5**.

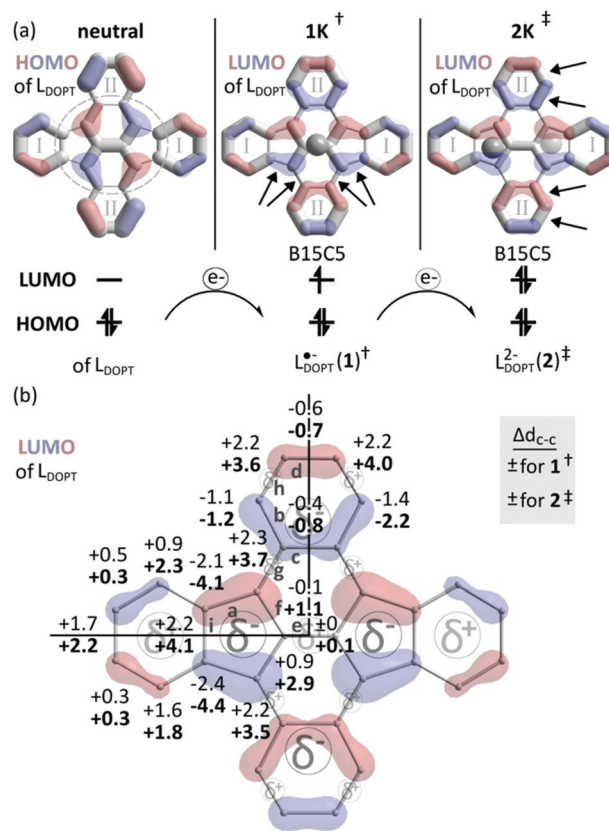


**Fig. 7** Schematic overview of the structural changes occurring by one electron reduction of DOPT. Its occupied molecular orbital (MO) is depicted in transparent mode (left: HOMO of  $L_{\text{DOPT}}$ ; middle and right: LUMO of DOPT; calculated at the B3LYP/6-31G\*\* level<sup>4,52</sup>). The thicker  $\text{C}_{\pi}-\text{C}_{\pi}$  bonds represent increased electron density in the bonding orbitals *i.e.*, decreasing bond length values and *vice versa* (red and blue color decode for regions of  $\psi^2$  of opposite sign). All MOs are plotted at the 90% probability level of the corresponding MO electron density ( $\psi^2$ ). The encircled position denotes the area of pronounced change and major electron concentration in  $[L_{\text{DOPT}}^{\cdot-}]$  and  $[L_{\text{DOPT}}^{2-}]$ . (b) Deviations  $\Delta d_{\text{C-C}}$  values in  $\pm$ pm are given for  $[L_{\text{DOPT}}^{\cdot-}]$  (top value<sup>†</sup>) and  $[L_{\text{DOPT}}^{2-}]$  (in bold<sup>‡</sup>) compared to  $L_{\text{DOPT}}$  (C2/c polymorph<sup>4</sup>) together with the areas of decreasing ( $\delta^-$ ) and increasing ( $\delta^+$ ) electron density;  $\psi^2$  is illustrated exclusively atop the  $\pi$ -plane for clarity.

electron density can be proposed for the isolated mono- and dianions of  $L_{\text{DOPT}}$  on the 5-membered ring positions (denoted as I) as well as on the tetracenic phenylenes (denoted as II, Fig. 7). A drastic decrease in bond lengths is observed (denoted as  $\delta^-$ , Fig. 7b), matching the calculated positions of up to  $-4.1$ – $-4.4$  pm for the peripheric  $\text{C}_{\pi}-\text{C}_{\pi}$  distances (a, Fig. 7b) of the five membered rings. For the tetracenic ring system,  $\text{Pn}_{\text{tet}}$ , a maximum of  $-1.2$ – $-2.2$  pm for the peripheric inner  $\text{C}_{\pi}-\text{C}_{\pi}$  bonds is observed (b, Fig. 7b). In contrast, an increase (denoted as  $\delta^+$ , Fig. 7b) by  $+4.1$  pm in bond lengths when going from  $[L_{\text{DOPT}}^{\cdot-}]$  in **1** to  $[L_{\text{DOPT}}^{2-}]$  in **2** is observed for the inner  $\text{C}_{\pi}-\text{C}_{\pi}$  bonds of  $\text{Pn}_{\text{peri}}$  (I) (i, Fig. 7b) and the outer periphery of  $\text{Pn}_{\text{tet}}$  (II) by  $+3.6$ – $+4.0$  pm (h, Fig. 7b). The peripheric tetracene positions (g, Fig. 7b) are altered by a maximum of  $+3.5$ – $+3.7$  pm and the inner naphthalenic bonds by *ca.*

+1.1|+2.9 pm (f, Fig. 7b). The outer peripheric phenylene bonds (I) are affected to a lesser extent. As a consequence, these bonds mainly increase by values of up to +2.3 pm. Twofold reduction of DOPT to the dianion [ $L_{DOPT}^{2-}$ ] in 2 (Fig. 7a, right) provokes an even more pronounced elongation, and contraction of the C–C bonds compared to its monoanion counterpart [ $L_{DOPT}^{-}$ ] in 1 respectively (Fig. 7a, middle).

## Experimental details

All syntheses were performed under an inert gas atmosphere of pretreated high purity argon (4.8, 99.998%) piped through a 4-column series arrangement filled with: (a) activated charcoal; (b) an activated BTS-copper catalyst (Sigma-Aldrich®); (c) activated molecular sieves, 3 Å; (d) SICAPENT® with an indicator (Merck). Hygroscopic benzo-15-crown-5-ether (B15C5) was synthesized from diethylene glycol dimethanesulfonate (DEGMS) with a modification of the literature protocol.<sup>53,54</sup> (\*) For application purpose, B15C5 was dissolved in dry THF (B15C5: 2.38 g in 40.0 mL; 0.222 mol L<sup>-1</sup>), degassed and stored static over activated molecular sieves (3 Å) for at least 1 week.

DOPT was synthesized as reported earlier by our group and was subsequently recrystallized from a hot THF solution.<sup>4,10</sup> All other chemicals were purchased and used as received. 1,2-Benzenediol (≥99%), cesium carbonate (99.5%), triethylamine (99%) and methanesulfonylchloride (99.50%) were obtained from Acros Organics; potassium (98%) from Alfa Aesar and diethylene glycol (≥99%) from Carl Roth. Tetrahydrofuran (THF), *N,N*-dimethylformamide (DMF), dimethylsulfoxide (DMSO), 1,4-dioxane, acetonitrile and dichloromethane were of technical grade and predried (1,4-dioxane and THF:<sup>55</sup> distilled over Na/benzophenone; DMF and DMSO: distilled over CaH<sub>2</sub>; and acetonitrile and CH<sub>2</sub>Cl<sub>2</sub>: distilled over P<sub>4</sub>O<sub>10</sub>), degassed and stored static over activated molecular sieves (3 Å/4 Å (CH<sub>2</sub>Cl<sub>2</sub>, DMSO)) prior to use. Pyridine was purchased from Merck (dried, SeccoSolv®, ≥99.9%). Deuterated THF-d<sub>8</sub> (99.50%) was purchased from Euriso-top®, dried on a potassium mirror under argon and then vacuum transferred.

Deuterated CHCl<sub>3</sub>-d<sub>1</sub> (99.8%) was purchased from Aldrich and used as received. Celite® was purchased from Sigma-Aldrich and predried at 300 °C in under high vacuum (<10<sup>-3</sup> mbar) for 2 h prior to use. Suitable crystals for structural analysis were obtained from a saturated THF solution under argon at -30 °C in sealed H-shaped flasks (see ESI†). DEGMS was crystallized from CH<sub>2</sub>Cl<sub>2</sub> at ambient temperature.

The X-ray diffraction data for DEGMS were collected on a STOE STADI IV 4-circle single-crystal diffractometer at ambient temperature. The crystal structure of DEGMS is reported in a private communication<sup>56</sup> in the Cambridge Structural Database, Refcode: ZIVRON; CCDC 968551. The X-ray diffraction data for the fully naked anions 1 and 2 were collected on, respectively, a Bruker AXS X8 Proteum diffractometer equipped with a Nonius FR591 copper rotating anode and a Bruker AXS Mach3 equipped with an Incoatec I $\mu$ S X-ray source at 100(2) K. The crystals were mounted on a MiTiGen loop using

degassed perfluorinated polyether. Structures were solved by direct methods (SHELXS) and refined by full-matrix least-squares (SHELXL).<sup>57</sup> Graphics of the molecules and unit cells were generated with the latest version of PLATON<sup>58</sup> and Diamond<sup>59</sup> software. All atomic displacement ellipsoids of the ORTEP<sup>47</sup> plots were drawn at the 50% probability level. Additional graphic details are given in the ESI.†

Due to the proven potent carcinogenic activity of some polyarenes, an uncontrolled release of PAHs constitutes a serious environmental contamination which is potentially hazardous for health.<sup>60</sup> Thus, handling and synthesis of PAHs has to be done with great care and any exposure should be precluded. In general, the use of any silicon based grease should be avoided due to the proven chance of irreversible incorporation of (H<sub>3</sub>C)<sub>2</sub>Si groups into the  $\pi$ -perimeter *via* reductive reaction with an alkaline metal.<sup>40</sup> Nonetheless, we never observed any competing reaction for DOPT during synthesis or significant disturbance of the reaction solution impeding crystal growth. The distillation of technical THF over active solvent-drying agents (*e.g.*, Na/K alloy, NaH, Na/benzophenone) is mandatory owing to the competing formation of adducts with the admixed stabilizer 2,6-di(*tert*-butyl)-4-methylphenol, as has been shown well by Bock *et al.*<sup>55</sup>

Note: The very limited solubility of the compounds (*e.g.*, in THF) together with their extremely high air and temperature sensitivity prevented their full spectroscopic characterization.

### Diethylene glycol dimethanesulfonate (DEGMS)

Triethylamine (43.9 mL, 32.0 g, 316 mmol; 1.5 eq.) was added to a mixture of diethylene glycol (20 mL, 22.4 g, 211 mmol; 1 eq.) in CH<sub>2</sub>Cl<sub>2</sub> (1.06 L; 0.2 M) at 0 °C. Methanesulfonylchloride (35.9 mL, 53.2 g, 464 mmol; 2.2 eq.) was added in small portions within 10 min and the reaction mixture was allowed to warm up to room temperature. After extraction with iced water (2 × 400 mL), aqueous HCl (10%, 2 × 400 mL), saturated Na<sub>2</sub>CO<sub>3</sub> (2 × 300 mL), brine (1 × 300 mL) and water, the organic layer was separated and dried with MgSO<sub>4</sub>. The solvent was removed *in vacuo* and the oily residue so obtained was solidified at -30 °C overnight. Subsequent recrystallization from CH<sub>2</sub>Cl<sub>2</sub> yielded pure and slightly hygroscopic dimesylate DEGMS (26.0 g, 99.1 mmol; 47% yield) as colorless prismatic crystals suitable for X-ray structural analysis. Atomic mass calculated for C<sub>6</sub>H<sub>14</sub>S<sub>2</sub>O<sub>7</sub>: 262.29 u; MS (70 eV): *m/z* (%): (EI) 263(1) [M<sup>+</sup>], 153(25) [M<sup>+</sup> - C<sub>2</sub>H<sub>5</sub>O<sub>3</sub>S], 123(100) [C<sub>3</sub>H<sub>7</sub>SO<sub>3</sub><sup>+</sup>], 79(55) [CH<sub>3</sub>SO<sub>2</sub><sup>+</sup>]; analysis calculated for C<sub>6</sub>H<sub>14</sub>S<sub>2</sub>O<sub>7</sub>: C, 27.45; H, 5.30. Found: C, 27.62; H 5.24. IR (ATR):  $\tilde{\nu}$  = 3030 (m), 2939 + 2888 + 2832 (w;  $\nu$ (C<sub>alkyl</sub>-H)), 1459 (m), 1330 (s;  $\nu$ (CH<sub>3</sub>-SO<sub>2</sub>-OR)), 1169 (s;  $\nu$ (CH<sub>3</sub>-SO<sub>2</sub>-OR)), 1134 + 1115 + 1073 (s + m + m;  $\nu$ (C-O-C)), 1014 (s), 974 (s), 935 (s), 914 (s), 810 (s), 733 (m), 555 (w), 525 (s), 480 (w), 460 (w), 447 (w) cm<sup>-1</sup>. <sup>1</sup>H-NMR (500 MHz, CHCl<sub>3</sub>-d<sub>1</sub>, 25 °C):  $\delta$  = 4.34 (t, <sup>3</sup>J(H<sub>2</sub>,H<sub>3</sub>) = 4.5 Hz, H<sub>2</sub>/H<sub>2</sub>'), 3.76 (dd, <sup>3</sup>J(H<sub>3</sub>,H<sub>2</sub>) = 4.5 Hz, 4H, H<sub>3</sub>/H<sub>3</sub>'), 3.00 (s, 6H, H<sub>1</sub>/H<sub>1</sub>') ppm. <sup>13</sup>C-NMR (500 MHz, CHCl<sub>3</sub>-d<sub>1</sub>, 25 °C):  $\delta$  = 69.02 (CH<sub>2</sub>, 2C, C<sub>3</sub>/C<sub>3</sub>'), 68.88 (CH<sub>2</sub>, 2C, C<sub>2</sub>/C<sub>2</sub>'), 37.46 (CH<sub>3</sub>, 2C, C<sub>1</sub>/C<sub>1</sub>') ppm.

### Benzo-15-crown-5-ether (B15C5)

Dry cesium carbonate (36.69 g, 112.6 mmol; 2.5 eq.) was added to 1,2-benzenediol (4.96 g, 45.0 mmol; 1 eq.) in degassed acetonitrile (1.0 L; 0.045 M), heated to reflux and stirred for 3 h. After cooling down to ambient temperature, a solution of the as-prepared DEGMS (11.80 g, 45.0 mmol; 1 eq.) in degassed acetonitrile (0.5 L; 0.09 M) was added in small portions (3 mL h<sup>-1</sup>). Subsequently, the mixture was refluxed for 48 h, cooled down and filtered over predried Celite®. The filtration residue was washed three times with additional CH<sub>2</sub>Cl<sub>2</sub> (each 300 mL) and the collected organic phase was concentrated *in vacuo*. The resulting residue was redissolved in fresh CH<sub>2</sub>Cl<sub>2</sub> and extracted with diluted aqueous HCl (1 M; 2 × 30 mL), brine (2 × 30 mL) and water (2 × 30 mL). The organic phase was dried with MgSO<sub>4</sub> and the solvent was removed *in vacuo*. Subsequent recrystallization from dry CH<sub>2</sub>Cl<sub>2</sub> under argon led to the precipitation of pure B15C5 as white hygroscopic needles (7.10 g, 26.5 mmol; 59% yield). IR (ATR):  $\tilde{\nu}$  = 3058 (w;  $\nu$ (C<sub>aryl</sub>-H)), 2940 + 2919 + 2856 (s;  $\nu$ (C<sub>alkyl</sub>-H)), 1591 (m), 1505 (s), 1450 (s), 1409 (w), 1360 (w), 1333 (m), 1297 (m), 1251 + 1228 (s;  $\nu$ (C<sub>aryl</sub>-O-C)), 1120 + 1091 + 1075 (s + s + m;  $\nu$ (C-O-C)), 1041 (s;  $\nu$ (C<sub>aryl</sub>-O-C)), 980 (w), 931 (s), 907 (m), 849 (m), 819 (w), 780 (m), 738 (s; 1,2-disubst.), 601 (w), 537 (w), 514 (w), 468 (w) cm<sup>-1</sup>. <sup>1</sup>H-NMR (500 MHz, DMSO-d<sub>6</sub>, 25 °C) = 6.96 (dd, 2H, H2/H2'), 6.89 (dd, 2H, H1/H1'), 4.04 (t, 4H, H3/H3'), 3.78 (t, 4H, H4/H4'), 3.64 (t, 8H, H5/H5'/H6/H6') ppm. <sup>13</sup>C-NMR (500 MHz, DMSO-d<sub>6</sub>, 25 °C) = 148.70 (C<sub>q</sub>, 2C, C2a), 121.23 (CH, 2C, C1/C1'), 114.19 (CH, 2C, C2/C2'), 70.44 (CH<sub>2</sub>, 2C, C6/C6'), 70.31 (CH<sub>2</sub>, 2C, C5/C5'), 69.04 (CH<sub>2</sub>, 2C, C4/C4'), 68.90 (CH<sub>2</sub>, 2C, C3/C3') ppm.

### Potassium bis(benzo-15-crown-5-ether) {[(B15C5-κ<sup>5</sup>O)<sub>2</sub>K<sup>+</sup>](L<sub>DOPT</sub><sup>2-</sup>)} (1)

A solution of DOPT (100 mg, 0.266 mmol; 1 eq.) in dry THF (20 mL) was reduced on an excess of finely vacuum-deposited potassium mirror (104 mg, 2.66 mmol; 10 eq.) for 2 hours at 0 °C. Ultrasonication supported the conversion. The reaction progress was accompanied by a quick color change from deep-blue to deep-red indicating the formation of the dianionic state [L<sub>DOPT</sub><sup>2-</sup>] of DOPT. The solution was filtered under argon over a thin layer of predried Celite® to remove finely dispersed potassium particles which are proven to be incompatible with the crown-ether.<sup>61-63</sup> An equimolar solution of additional neutral DOPT (100 mg, 0.266 mmol) was transferred to the filtrate. The reaction mixture was stirred for 1 h to ensure equilibration to the deep-green radical monoanionic state [L<sub>DOPT</sub><sup>•-</sup>]. Addition of the predried solution (\*) of B15C5 (143 mg, 0.53 mmol; 2 eq.) in THF (2.4 mL; 0.222 mol L<sup>-1</sup> in THF), and storage at -30 °C for 7 days yielded dark-green rhombic crystals suitable for X-ray structural analysis.

### Di-potassium bis(benzo-15-crown-5-ether) {[(B15C5-κ<sup>5</sup>O)<sub>2</sub>K<sup>+</sup>]<sub>2</sub>(L<sub>DOPT</sub><sup>2-</sup>)} (2)

Analogous to the above procedure, addition of the B15C5-solution was carried out directly to the filtered deep-red solution of

the dianionic state [L<sub>DOPT</sub><sup>2-</sup>] of DOPT. The encapsulating agent B15C5 (285 mg, 1.06 mmol; 4 eq. in 4.8 mL THF) was injected under vigorous stirring accompanied by a slight change in color from deep-red to light-red. Finally, the reaction flask was stored free of vibration at -30 °C for several days. Red rhombic crystals suitable for X-ray structural analysis were separated from the pale-red solution, indicative of an almost quantitative formation of the solvent-separated ion triad 2.

## Conclusions

The structural results of the radical monoanion {[(B15C5-κ<sup>5</sup>O)<sub>2</sub>K<sup>+</sup>](L<sub>DOPT</sub><sup>•-</sup>)} (1) (Fig. 1) and the dianion {[(B15C5-κ<sup>5</sup>O)<sub>2</sub>K<sup>+</sup>]<sub>2</sub>(L<sub>DOPT</sub><sup>2-</sup>)}THF<sub>solv</sub> (2) (Fig. 3) of 5,6:11,12-di-*o*-phenylene-tetracene (DOPT, L<sub>DOPT</sub>; Fig. 7) extended our work on the reduction behavior of the newly accessible polycyclic aromatic hydrocarbon DOPT. Reduction of DOPT with elemental potassium completed our studies on the systematic influence of the hard- and softness of the employed reducing agent (M = Li, Na, K) on the shape of a charged carbon skeleton in the solvent-separated ion-pairs of this ligand. By using the poly-*O*-macrocycle, benzo-15-crown-5-ether (B15C5) full cation/anion charge separation has been achieved, whereby encapsulation of the K<sup>+</sup> into the more rigid cage of [(B15C5-κ<sup>5</sup>O)<sub>2</sub>K<sup>+</sup>] results in a (κ<sup>10</sup>O) coordination geometry. With respect to the recently reported dianions of DOPT, containing separated (κ<sup>6</sup>O)-capsules of [(DME-κ<sup>2</sup>O)<sub>3</sub>Li<sup>+</sup>], [(DME-κ<sup>2</sup>O)<sub>3</sub>Na<sup>+</sup>] and [(diglyme-κ<sup>3</sup>O)<sub>2</sub>Na<sup>+</sup>], the full sandwich coordination in [(B15C5-κ<sup>5</sup>O)<sub>2</sub>K<sup>+</sup>] described herein proves an exceptionally high donor capability of the DOPT π-perimeter which becomes possible under full charge separation. For all (κ<sup>6</sup>O)-geometries observed, the structural perturbation of the planar DOPT is distinct and can be attributed to electrostatic long range forces between the separated opposite charges (Fig. 6).

## Conflicts of interest

There are no conflicts to declare.

## Notes and references

- J. E. Anthony, *Angew. Chem., Int. Ed.*, 2008, **47**, 452–483.
- L. Torsi, M. Magliulo, K. Manoli and G. Palazzo, *Chem. Soc. Rev.*, 2013, **42**, 8612–8628.
- G. Dai, J. Chang, W. Zhang, S. Bai, K.-W. Huang, J. Xu and C. Chi, *Chem. Commun.*, 2015, **51**, 503–506.
- T. Wombacher, A. Gassmann, S. Foro, H. von Seggern and J. J. Schneider, *Angew. Chem., Int. Ed.*, 2016, **55**, 6041–6046.
- Z. Xu, *Coord. Chem. Rev.*, 2006, **250**, 2745–2757.
- M. M. Ahmida and S. H. Eichhorn, *ECS Trans.*, 2010, **25**, 1–10.
- L. Muccioli, C. Zannoni and D. Beljonne, *Chem. Mater.*, 2011, **23**, 591–609.

- 8 C. Melero, R. P. Herrera, A. Guijarro and M. Yus, *Chem. – Eur. J.*, 2007, **13**, 10096–10107.
- 9 C. Näther, H. Bock, Z. Havlas and T. Hauck, *Organometallics*, 1998, **17**, 4707–4715.
- 10 T. Wombacher, S. Foro and J. J. Schneider, *Eur. J. Org. Chem.*, 2016, 569–578.
- 11 T. Wombacher, R. Goddard, C. W. Lehmann and J. J. Schneider, *Chem. Commun.*, 2017, **53**, 7030–7033.
- 12 T. Wombacher, R. Goddard, C. W. Lehmann and J. J. Schneider, *Dalton Trans.*, 2017, **46**, 14122–14129.
- 13 A. V. Zabula, N. J. Sumner, A. S. Filatov, S. N. Spisak, V. M. Grigoryants and M. A. Petrukhina, *Eur. J. Inorg. Chem.*, 2012, 4675–4683.
- 14 H. Bock, Z. Havlas, K. Gharagozloo-Hubmann, S. Holl and M. Sievert, *Angew. Chem., Int. Ed.*, 2003, **42**, 4385–4389.
- 15 A. S. Paraskar, A. R. Reddy, A. Patra, Y. H. Wijsboom, O. Gidron, L. J. W. Shimon, G. Leitun and M. Bendikov, *Chem. – Eur. J.*, 2008, **14**, 10639–10647.
- 16 A. V. Zabula, S. N. Spisak, A. S. Filatov, V. M. Grigoryants and M. A. Petrukhina, *Chem. – Eur. J.*, 2012, **18**, 6476–6484.
- 17 A. V. Zabula, A. S. Filatov, J. Xia, R. Jasti and M. A. Petrukhina, *Angew. Chem., Int. Ed.*, 2013, **52**, 5033–5036.
- 18 H. Bock, S. Holl and M. Sievert, *Z. Naturforsch., B: Chem. Sci.*, 2000, **55**, 1163–1178.
- 19 D. A. Walker, B. Kowalczyk, O. De and B. A. Grzybowski, *Nanoscale*, 2011, **3**, 1316–1344.
- 20 H. Bock, R. F. C. Claridge, C. Bogdan, M. Sievert and V. Krenzel, *Helv. Chim. Acta*, 2001, **84**, 1227–1242.
- 21 H. Bock, M. Ansari, N. Nagel and R. F. C. Claridge, *J. Organomet. Chem.*, 1996, **521**, 51–63.
- 22 H. Bock, M. Ansari, N. Nagel and R. F. C. Claridge, *J. Organomet. Chem.*, 1995, **501**, 53–60.
- 23 A. V. Zabula, S. N. Spisak, A. S. Filatov, A. Y. Rogachev, R. Clérac and M. A. Petrukhina, *Chem. Sci.*, 2016, **7**, 1954–1961.
- 24 S. N. Spisak, A. V. Zabula, M. V. Ferguson, A. S. Filatov and M. A. Petrukhina, *Organometallics*, 2013, **32**, 538–543.
- 25 S. N. Spisak, N. J. Sumner, A. V. Zabula, A. S. Filatov, A. Y. Rogachev and M. A. Petrukhina, *Organometallics*, 2013, **32**, 3773–3779.
- 26 K. Gharagozloo-Hubmann, *Johann Wolfgang Goethe-Universität Frankfurt am Main*, 2000.
- 27 H. Bock, C. Nather and Z. Havlas, *J. Am. Chem. Soc.*, 1995, **117**, 3869–3870.
- 28 H. Sjoerd, *Chem. – Eur. J.*, 1999, **5**, 1852–1861.
- 29 M. T. Reetz, S. Hutte, R. Goddard and U. Minet, *J. Chem. Soc., Chem. Commun.*, 1995, 275–277.
- 30 S. Harder, M. H. Prosenc and U. Rief, *Organometallics*, 1996, **15**, 118–122.
- 31 M. L. Cole, C. Jones and P. C. Junk, *J. Chem. Soc., Dalton Trans.*, 2002, 896–905.
- 32 D. Eisenberg and R. Shenhar, *Wiley Interdiscip. Rev.: Comput. Mol. Sci.*, 2012, **2**, 525–547.
- 33 P. R. Mallinson and M. R. Truter, *J. Chem. Soc., Perkin Trans. 2*, 1972, **12**, 1818–1823.
- 34 S. Kriek, H. Görls and M. Westerhausen, *Organometallics*, 2010, **29**, 6790–6800.
- 35 H. Bock, C. Arad, C. Nather and Z. Havlas, *J. Chem. Soc., Chem. Commun.*, 1995, 2393–2394.
- 36 T. Scott, B. Ooro, D. J. Collins, M. Shatruk, A. Yakovenko, K. R. Dunbar and H.-C. Zhou, *Chem. Commun.*, 2009, 65–67.
- 37 H. Bock, K. Gharagozloo-Hubmann, M. Sievert and T. Prisner, *Nat.*, 2000, **404**, 267–269.
- 38 H. Bock, A. John, C. Näther, Z. Havlas and E. Mihokova, *Helv. Chim. Acta*, 1994, **77**, 41–50.
- 39 M. Saito, Y. Hashimoto, T. Tajima, K. Ishimura, S. Nagase and M. Minoura, *Chem. – Asian J.*, 2012, **7**, 480–483.
- 40 H. Bock, M. Sievert, C. L. Bogdan and B. O. Kolbesen, *Organometallics*, 1999, **18**, 2387–2389.
- 41 I. L. Fedushkin, A. N. Lukoyanov, S. Dechert and H. Schumann, *Eur. J. Inorg. Chem.*, 2004, 2421–2424.
- 42 W. Jost, M. Adam, V. Enkelmann and K. Müllen, *Angew. Chem.*, 1992, **104**, 883–884.
- 43 H. Bock, *Nachr. Chem.*, 2001, **49**, 18–21.
- 44 N. L. Nock, D. Tang, A. Rundle, C. Neslund-Dudas, A. T. Savera, C. H. Bock, K. G. Monaghan, A. Koprowski, N. Mitrache, J. J. Yang and B. A. Rybicki, *Cancer Epidemiol. Biomarkers Prev.*, 2007, **16**, 1236–1245.
- 45 H. Bock, K. Ruppert, C. Nather, Z. Havlas, H. Herrmann, C. Arad, I. Gobel, A. John, J. Meuret, S. Nick, A. Rauschenbach, W. Seitz and T. Vaupel, *Angew. Chem.*, 1992, **104**, 564–595.
- 46 A. S. Filatov, N. J. Sumner, S. N. Spisak, A. V. Zabula, A. Y. Rogachev and M. A. Petrukhina, *Chem. – Eur. J.*, 2012, **18**, 15753–15760.
- 47 C. K. Johnson, Oak Ridge National Laboratory, Report ORNL-5138, O, 1976.
- 48 M. Bartošková and Z. Friedl, *Cent. Eur. J. Energ. Mater.*, 2013, **10**, 103–112.
- 49 R. F. W. Bader, M. T. Carroll, J. R. Cheeseman and C. Chang, *J. Am. Chem. Soc.*, 1987, **109**(26), 7968–7979.
- 50 R. J. Feldmann, D. H. Bingt, B. C. Furief and B. Furief, *Proc. Natl. Acad. Sci. U. S. A.*, 1978, **75**, 5409–5412.
- 51 R. D. Shannon, *Acta Crystallogr.*, 1976, **32**, 751–767.
- 52 C. M. Murata, Y. Sugano, A. Wakamiya and Y. Murata, *Angew. Chem., Int. Ed.*, 2015, **54**, 9308–9312.
- 53 R. E. Hanes, C. Lee, S. N. Ivy, A. Palka and R. A. Bartsch, *Arch. Org. Chem.*, 2010, **7**, 238–248.
- 54 J. S. Bradshaw and P. E. Stott, *Heterocycles*, 1981, **75**, 179–182.
- 55 H. Bock, R. Dienelt, C. Näther and Z. Havlas, *Chem. Ber.*, 1997, **130**, 1533–1537.
- 56 J. W. Nail, R. D. Gandour and F. R. Fronczek, 2014.
- 57 G. M. Sheldrick, *Acta Crystallogr., Sect. A: Found. Crystallogr.*, 2008, 112–122.
- 58 A. L. Spek, *Acta Crystallogr., Sect. D: Biol. Crystallogr.*, 2009, **65**, 148–155.
- 59 W. T. Pennington, *J. Appl. Crystallogr.*, 1999, **32**, 1028–1029.

- 60 C. A. Menzie, B. B. Potocki and J. Santodonato, *Environ. Sci. Technol.*, 1992, **26**, 1278–1284.
- 61 Z. Grobelny, A. Stolarzewicz, M. Szczepanski and M. Sokol, *Curr. Org. Chem.*, 2008, **12**, 1040–1049.
- 62 Z. Grobelny, A. Stolarzewicz and A. Maercker, *J. Organomet. Chem.*, 2001, **628**, 65–70.
- 63 Z. Grobelny, A. Stolarzewicz, M. Sokol, J. Grobelny and H. Janeczek, *J. Phys. Chem.*, 1992, **96**, 5193–5196.